

Research paper

Vibrational resonance in a harmonically trapped potential system

K. Abirami^a, S. Rajasekar^{a,*}, M.A.F. Sanjuan^b^aSchool of Physics, Bharathidasan University, Tiruchirappalli, 620 024, Tamilnadu, India^bNonlinear Dynamics, Chaos and Complex Systems Group, Departamento de Física, Universidad Rey Juan Carlos, Tulipán s/n, M'ostoles, 28933, Madrid, Spain

ARTICLE INFO

Article history:

Received 18 May 2016

Revised 26 November 2016

Accepted 1 December 2016

Available online 2 December 2016

Keywords:

Harmonically trapped potential

Biharmonic force

Vibrational resonance

ABSTRACT

We report our investigation of role of shape of a harmonically trapped potential system driven by a biharmonic external force with two widely different frequencies ω and Ω with $\Omega \gg \omega$ on vibrational resonance. The potential is capable of generating odd number of potential wells depending upon the values of the parameters in the potential function. Applying a theoretical approach we obtain an analytical expression for the response amplitude Q at the low-frequency ω . The response amplitude exhibits multiple peaks and approaches a non-zero limiting value when the amplitude of the high-frequency force is varied. We explain the mechanism of observed resonance dynamics. We bringout the effect of number of potential wells on the resonance behaviour.

© 2016 Published by Elsevier B.V.

1. Introduction

Nonlinear systems are ubiquitous and certain types of them are capable of showing a variety of phenomena. Among the various phenomena exhibited by nonlinear systems nonlinear resonances are fundamental importance in basic and applied sciences. The forced resonance (resonance induced by an additive external periodic force) [1–4] and parametric resonance [4,5] occur in both linear and nonlinear systems. The stochastic resonance [6,7], coherence resonance [8,9], auto resonance [10,11], ghost resonance [12–14], chaos resonance [15] and vibrational resonance [4,16–20] can be realized only in nonlinear systems. The present paper is concerned with vibrational resonance. Consider a nonlinear system driven by two periodic signals of widely different frequencies, say ω and Ω with $\Omega \gg \omega$. Assume that in the absence of high-frequency (Ω) force, the response amplitude of the system at the low-frequency ω is weak. When the amplitude g of the high-frequency force is varied from a small value, the response amplitude at the low-frequency ω displays resonance at one or more values of g . This high-frequency force induced resonance at the low-frequency is termed as vibrational resonance.

Gitterman [17] and Blekhman and Landa [18] developed theoretical methods for analyzing vibrational resonance. Since then this resonance phenomenon has been investigated theoretically, numerically and experimentally in many oscillators, excitable systems, maps, networks and time-delayed systems. It is important to investigate the role of shape of potentials on vibrational resonance. In this direction, the occurrence of vibrational resonance has been examined in bistable [16–18,21–24], monostable [25], asymmetric [26], spatially periodic [27] and spatially extended single-well [28] potentials systems. It has also been analyzed in an excitable system [29] and in a system with signum nonlinearity [30].

* Corresponding author. Fax: +914312407093.

E-mail addresses: nk.abirami@gmail.com (K. Abirami), rajasekar@cndd.bdu.ac.in (S. Rajasekar), miguel.sanjuan@urjc.es (M.A.F. Sanjuan).

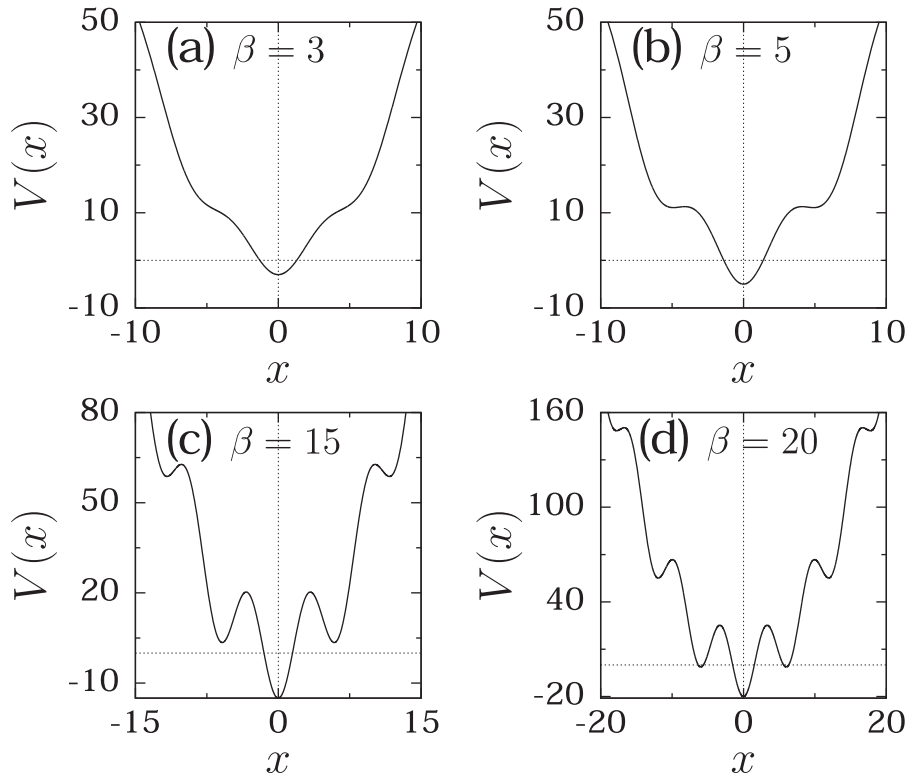


Fig. 1. The shape of the potential (1) with $\omega_0^2 = 1$ and for four values of β .

Motivated by the above consideration, in the present paper we consider the damped nonlinear system with harmonically trapped potential

$$V = \frac{1}{2}\omega_0^2x^2 - \beta \cos x, \quad \omega_0^2, \beta > 0 \tag{1}$$

and driven by the biharmonic force. The equation of motion of the system of our interest is given by

$$\ddot{x} + d\dot{x} + \omega_0^2x + \beta \sin x = f \cos \omega t + g \cos \Omega t, \quad \Omega \gg \omega. \tag{2}$$

In Eq. (2) $\Omega \gg \omega$ and $d > 0$. A feature of the potential given by Eq. (1) is that it can generate odd number of potential wells of different depths depending upon the values of the parameters ω_0^2 and β . Fig. 1 shows the shape of the potential for four fixed values of β for $\omega_0^2 = 1$. The multistable potential generated experimentally in an experimental torsion balance oscillator [31] resembles that of the multistable potential given by Eq. (1) for larger values of β . It can be used as an alternative potential for the typical polynomial potentials $V(x)$ used for representing potentials with single-well, triple-well and other odd-number of wells.

Here, we are interested in investigating the role of shape of the potential given by Eq. (1) on vibrational resonance. Applying a theoretical treatment, we obtain an approximate analytical expression for the response amplitude (Q) at the low-frequency ω . The theoretical prediction is found to be in good agreement with the numerically computed Q . Even for the single-well case of the system the response amplitude shows number of resonance peaks approaching a limiting value. We describe the mechanism of observed variation of Q .

The organization of the paper is as follows. To start with in Section 2 we present the effect of the parameter β on the shape of the potential and the number of equilibrium points. The number of equilibrium points depends on β . In Section 3 first we assume that the solution of the system consists of two frequencies ω and Ω and obtain an approximate linear equation of motion for the component of solution with period $2\pi/\omega$ or the frequency ω . We find an analytical expression for $Q(\omega)$. We compare the theoretical Q with the numerically computed Q . Then we analyse the occurrence of vibrational resonance for the cases of the system with single-well. Vibrational resonance of the system with three and five wells is discussed in Section 4. In Section 5 we present the effect of initial conditions on $Q(\omega)$ for $\beta = 15$. Finally, Section 6 contains conclusion.

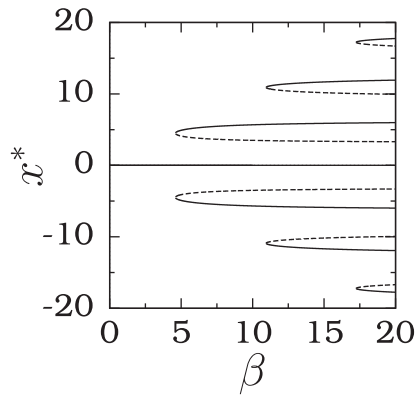


Fig. 2. x^* (equilibrium points) versus the parameter β of the system (2) in the absence of biharmonic force. Here $\omega_0^2 = 1$ and x^* is independent of d .

2. Effect of β on the shape of the potential and the number of equilibrium points

The shape of the potential and the number of local minima and maxima of the potential (number of equilibrium points of the system (2) in the absence of the external periodic force) depends on the parameters ω_0^2 and β . Here, we consider the effect of β . The potential is symmetrical about $x = 0$. As shown in Fig. 1 for $\omega_0^2 = 1$ the potential has odd number of wells depending on the value of β . The minima or the maxima of the potential (1) are the x -component of the equilibrium points ($x^*, \dot{x}^* = y^* = 0$) of the system (2) in the absence of the external driving biharmonic force. They are the roots of the equation

$$\omega_0^2 x^* + \beta \sin x^* = 0. \tag{3}$$

$x^* = 0$ is always a root. For fixed values of ω_0^2 and β from Eq. (3) we notice that $|x^*| \leq \beta/\omega_0^2$. Further, if x^* is a root of (3) then $-x^*$ is also a root.

It is difficult to find an analytical expression for x^* from Eq. (3). However, we can determine all the roots of Eq. (3) numerically, by employing Newton-Raphson method. The stability determining eigenvalues are given by

$$\lambda_{\pm} = \frac{1}{2} \left[-d \pm \sqrt{d^2 - 4\omega_0^2 - 4\beta \cos x^*} \right]. \tag{4}$$

An equilibrium point is stable if $\lambda_{\pm} < 0$ otherwise unstable. We numerically computed all real values of x^* and the stability of the equilibrium point $s(x^*, \dot{x}^* = 0)$. Fig. 2 presents the numerically computed x^* as a function of β for $\omega_0^2 = 1$. The stable and unstable equilibrium points are represented by continuous and dashed curves, respectively. $(x^*, \dot{x}^*) = (0, 0)$ is always stable. For $0 < \beta \leq 3\pi/2$, $(0, 0)$ is the only equilibrium point and the associated $V(x)$ is a single-well potential (Fig. 1a, where $\beta = 3$). For $3\pi/2 < \beta \leq 7\pi/2$ there are five equilibrium points with three being stable and the remaining two being unstable. The corresponding potential (Fig. 1b where $\beta = 5$) $V(x)$ is a three-well potential. Depending on the value of β the system has $4n - 3$, $n = 1, 2, 3, \dots$ number of equilibrium points while $V(x)$ has $2n - 1$, $n = 1, 2, \dots$ wells. The change in the number of equilibrium points and the number of wells in the potential occur at $\beta = (4n - 1)\pi/2$, $n = 1, 2, \dots$

3. Analysis of vibrational resonance

3.1. Analytical expression for the response amplitude

Due to the choice of ω and Ω as $\Omega \gg \omega$, that is ω and Ω are widely separated, it is reasonable to assume that the solution of Eq. (2) consists of a slow variable X with period $2\pi/\omega$ and a fast variable ψ with period $2\pi/\Omega$. Substituting $x = X + \psi$ in Eq. (2) we get

$$\ddot{X} + \ddot{\psi} + d\dot{X} + d\dot{\psi} + \omega_0^2 X + \omega_0^2 \psi + \beta \sin X \cos \psi + \beta \cos X \sin \psi = f \cos \omega t + g \cos \Omega t. \tag{5}$$

Adding and subtracting $\beta \sin X \langle \cos \psi \rangle$ and $\beta \cos X \langle \sin \psi \rangle$ in Eq. (5), where

$$\langle \cos \psi \rangle = \frac{1}{\Delta} \int_0^{\Delta} \cos \psi(t) dt, \quad \langle \sin \psi \rangle = \frac{1}{\Delta} \int_0^{\Delta} \sin \psi(t) dt \tag{6}$$

with $\Delta = 2\pi/\Omega$, we arrive the equations for slow and fast motions as

$$\ddot{X} + d\dot{X} + \omega_0^2 X + \beta \langle \cos \psi \rangle \sin X + \beta \langle \sin \psi \rangle \cos X = f \cos \omega t \tag{7}$$

and

$$\ddot{\psi} + d\dot{\psi} + \omega_0^2 \psi + \beta (\cos \psi - \langle \cos \psi \rangle) \sin X + \beta (\sin \psi - \langle \sin \psi \rangle) \cos X = g \cos \Omega t, \tag{8}$$

respectively. As ψ is a rapidly varying function of time, we can approximate Eq. (8) as $\ddot{\psi} = g \cos \Omega t$ giving $\psi = \mu \cos \Omega t$ where $\mu = -g/\Omega^2$. Using this ψ in Eq. (6) we get $\langle \cos \psi \rangle = J_0(\mu)$ and $\langle \sin \psi \rangle = 0$ where J_0 is zeroth-order Bessel function [32,33] with the argument μ . Then Eq. (7) becomes

$$\ddot{X} + d\dot{X} + \omega_0^2 X + \beta J_0(\mu) \sin X = f \cos \omega t. \tag{9}$$

Eq. (9) is the equation of motion of a particle with the effective potential,

$$V_{\text{eff}} = \frac{1}{2} \omega_0^2 X^2 - \beta J_0 \cos X \tag{10}$$

subjected to linear damping and the driving force $f \cos \omega t$. Slow motion takes place about the stable equilibrium points of the unforced system (9). The X -component of the equilibrium points are the roots of the equation

$$\omega_0^2 X^* + \beta J_0 \sin X^* = 0. \tag{11}$$

The roots of Eq. (11) can be determined by using Newton–Raphson method. Then the linear equation for the deviation $Y = X - X^*$ of the slow variable from X^* obtained from Eq. (9) is

$$\ddot{Y} + d\dot{Y} + \omega_r^2 Y = f \cos \omega t, \tag{12}$$

where

$$\omega_r^2 = \omega_0^2 + \beta J_0 \cos X^*. \tag{13}$$

In Eq. (13) ω_r is resonant frequency of oscillation of the slow variable. Therefore, X^* in Eq. (13) is the X -component of the stable equilibrium point ($X^*, \dot{X}^* = 0$). In the long time limit, the solution of Eq. (12) is $Y = Q f \cos(\omega t + \phi)$ where

$$Q = \frac{1}{\sqrt{S}}, \quad S = (\omega_r^2 - \omega^2)^2 + d^2 \omega^2 \tag{14}$$

and

$$\phi = \tan^{-1} \left(\frac{d\omega}{\omega^2 - \omega_r^2} \right). \tag{15}$$

Q is termed as the response amplitude of the system (2) at the low-frequency ω of the input signal.

3.2. Numerical calculation of Q

In order to compare the theoretically calculated Q we numerically integrate Eq. (2) using the fourth-order Runge–Kutta method with step size $(2\pi/\omega)/1000$. After leaving a sufficient transient we calculate Q using

$$Q = \sqrt{Q_s^2 + Q_c^2}/f, \tag{16a}$$

where

$$Q_s = \frac{2}{nT} \int_0^{nT} x(t) \sin \omega t dt, \tag{16b}$$

$$Q_c = \frac{2}{nT} \int_0^{nT} x(t) \cos \omega t dt, \tag{16c}$$

with $T = 2\pi/\omega$ and $n = 500$.

3.3. The analysis of the response amplitude $Q(\omega)$

We fix the values of the parameters as $d = 0.5$, $\omega_0^2 = 1$, $f = 0.1$, $\omega = 1$ and $\Omega = 10\omega$. First, we choose $\beta = 3$ for which $V(x)$ is a single-well potential as shown in Fig. 1a. We treat g as the control parameter. For a fixed value of Ω the quantity J_0 is a function of g . On the other hand, for a fixed value of ω_0^2 we note that X^* and ω_r^2 are functions of J_0 and β , that is functions of g and β . X^*, J_0 and ω_r^2 are functions of g . Fig. 3 depicts the variation of X^* with g for $\omega_0^2 = 1$ and $\beta = 3$. For $0 < g \leq 325$ and $g > 444$ $X_0^* = 0$ is the only equilibrium point and is stable. For $325 < g \leq 444$ there are three equilibrium points: $X_0^* = 0$ is unstable while the other two are stable. In calculating ω_r^2 and then Q we use $X_0^* = 0$ for $0 < g \leq 325$ and $g > 444$. For $325 < g \leq 444$ $X^* \neq 0$ is used for calculating Q . When g is varied the quantity J_0 , ω_r^2 and Q vary. From Eq. (14) it is evident that Q becomes a maximum when $|\omega_r^2 - \omega^2|$ becomes a minimum. We vary g from a small value and compute theoretical Q from Eq. (14), numerical Q from Eq. (16) and quantity $|\omega_r^2 - \omega^2|$. The results are presented in Fig. 4. There are many interesting results. The theoretical Q closely matches with the numerically computed Q . The Q oscillates with g , however, it is not a damped oscillation. Q not decays to zero in the limit of $g \rightarrow \infty$. Rather Q displays a number of resonance peaks and approaches a nonzero limiting value. We explain the variation of Q with g using the quantities $|\omega_r^2 - \omega^2|$ and J_0 .

In Fig. 4b we note that J_0 exhibits damped oscillation, becomes zero at certain values of g and $J_0 \rightarrow 0$ as $g \rightarrow \infty$. For finite values of g , whenever $J_0 = 0$ from Eq. (13) we find that $\omega_r^2 = \omega_0^2 = 1 (= \omega^2)$. In this case from Eq. (14) we have

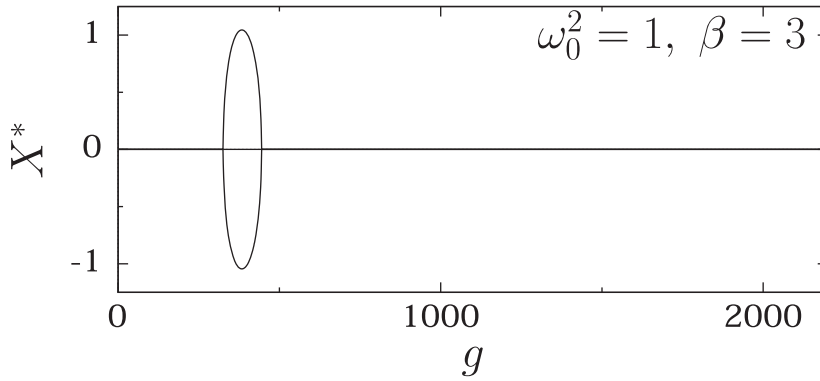


Fig. 3. Plot of X^* as a function of g for $\omega_0^2 = 1$, $\beta = 3$ of the unforced case of the system (9).

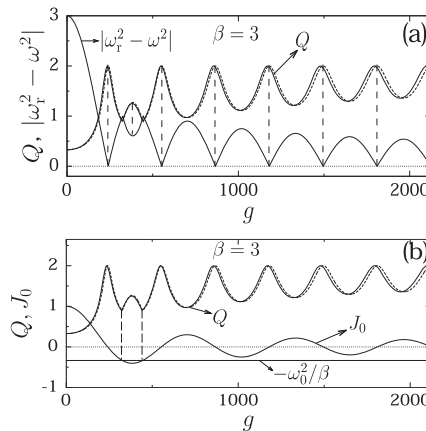


Fig. 4. (a) Variation of Q and $|\omega_r^2 - \omega^2|$ and (b) Q and J_0 as a function of the control parameter g for $\beta = 3$, $d = 0.5$, $f = 0.1$, $\omega_0^2 = 1$, $\omega = 1$ and $\Omega = 10\omega$. The theoretical and numerically calculated values of Q are represented by continuous and dashed curves, respectively.

$Q = 1/d\omega = 2$. For other values of g the quantity $(\omega_r^2 - \omega^2)^2 \neq 0$ and hence $Q < 2$. That is, the maximum value of Q is $1/d\omega$ and this happens whenever the resonant frequency ω_r matches with the frequency ω of the low-frequency force. Because J_0 crosses the value 0 number of times before becoming always negligibly small, there are number of resonance peaks of Q before approaching a limiting value. This is the source for number of resonance peaks of Q .

We need to account the second resonance in Fig. 4a. The value of Q at the second resonance is lower than the value of it at other resonance peaks. Consider the interval $g \in [g_1 = 325, g_2 = 445]$ within which second resonance occurs. In this interval of g the quantity $J_0 < -\omega_0^2/\beta$ and there three are equilibrium points: $X_0^* = 0$, $X_{\pm}^* \neq 0$. $X_0^* = 0$ is unstable while X_{\pm}^* are stable. Slow oscillation occurs about X_{\pm}^* . Further, in the above interval of g we have $\omega_r^2 - \omega^2 (= \omega_r^2 - \omega_0^2) = -\beta J_0 \cos X_{\pm}^*$. At $g = g_1$ and $g = g_2$ we find $X^* = 0$ in the expression for ω_r^2 , $J_0 = -\omega_0^2/\beta$, $\omega_r^2 = \omega_0^2 - (\beta\omega_0^2/\beta) = 0$, $|\omega_r^2 - \omega^2| = \omega^2 = 1$ and $Q = 1$. Between g_1 and g_2 , $J_0 \cos X_{\pm}^*$, varies with g and moreover both J_0 and $\cos X_{\pm}^*$ have a minimum at $g = 384$. At this value of g the quantity $|\omega_r^2 - \omega^2|$ has a local minimum as shown in Fig. 4a. That is, when g is varied from g_1 , $|\omega_r^2 - \omega^2|$ decreases from the value 1 (so that Q increases from the value 1), reaches a local minimum with the value $\neq 0$ at $g = 384$ (hence Q becomes locally maximum with a value < 2) and then increases (Q decreases) with further increase in the value of g . The observation is that when $J_0 < -\omega_0^2/\beta$ and $|\omega_r^2 - \omega^2|$ has a local minimum with a value $\neq 0$ then there will be a resonance with a value less than $1/(d\omega)$.

Next, we describe the change in the shape of the effective potential V_{eff} and the change in the center of the slow orbit. In Fig. 3 we observe that $X_0^* = 0$ is the only root of Eq. (11) for $0 < g \leq 325$ and $g > 444$. In this interval of g , $V_{\text{eff}}(x)$ is a single-well potential while for $325 < g \leq 444$ there are three X^* and the potential V_{eff} is a double-well potential. The double-well potential occurs when $J_0 < -\omega_0/\beta$. If there is a change in the number of wells in the potential at, say, g_1 and g_2 then there is a resonance at a value of g between g_1 and g_2 . What is the effect of change in the number of wells of the potential V_{eff} on $X(t)$? If V_{eff} is a single-well then there is a slow orbit centered about $X_0^* = 0$. This is the case for $0 < g \leq 325$ and $g > 444$. For $325 < g \leq 444$ from Fig. 3 as noted earlier the potential is a double-well in which $X_0^* = 0$ is the maximum of the potential while $X_{\pm}^* \neq 0$ are the two local minima. $X(t)$ occurs about X_{\pm}^* . That is, there are two distinct stable solutions $X(t)$, one about X_+^* and another about X_-^* .

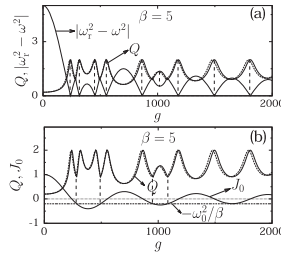


Fig. 5. (a) Q and $|\omega_F^2 - \omega^2|$ versus g and (b) Q and J_0 versus g for the system (2) for $d = 0.5$, $f = 0.1$, $\omega_0^2 = 1$, $\omega = 1$, $\Omega = 10\omega$ and $\beta = 5$. The theoretical and numerical values of Q plotted in continuous and dashed lines, respectively.

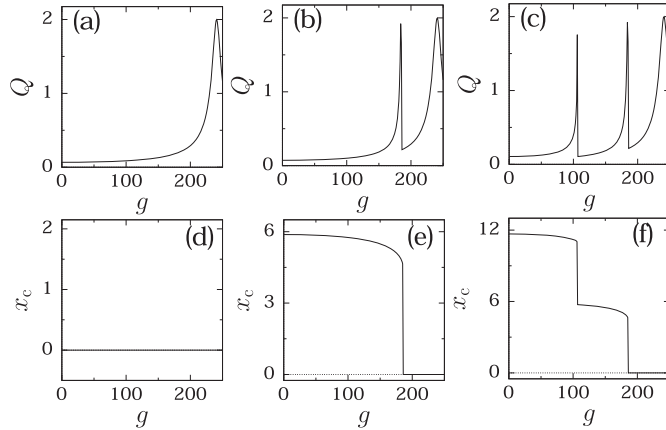


Fig. 6. Variation of Q with g for three initial conditions with $\beta = 15$. (a) $(x(0), \dot{x}) = (0, 0)$, $x(0) = 0$ is the minimum of the MW. (b) $(x(0), \dot{x}) = (5.88, 0)$, $x(0) = 5.88$ is the minimum of the RWAMW. (c) $(x(0), \dot{x}) = (11.67, 0)$, $x(0) = 11.67$ is the minimum of the RMW. (d-f) Variation of center of x, x_c , as a function of g corresponding to the subplots a, b, c, respectively.

4. Vibrational resonance for $\beta = 5$ and $\beta = 15$

In this section we analyse the occurrence of vibrational resonance for the cases of the potential with three and five wells.

4.1. Potential with three wells ($\beta = 5$)

For $\beta = 5$ the potential $V(x)$ has a three-well shape. Fig. 5 shows the variation of Q , $|\omega_F^2 - \omega^2|$ and J_0 as a function of g where $X^* = X_0^* = 0$. Here also Q displays a number of resonance peaks and approaches the limiting value 2. The values of Q at second and third resonance peaks are 2 and these two resonance peaks occur when $|\omega_F^2 - \omega^2| = 0$ with $J_0 < -\omega_0^2/\beta$. The sixth resonance peak has a value less than 2. It occurs at the local minimum of J_0 with $J_0 < -\omega_0^2/\beta$ and $|\omega_F^2 - \omega^2|$ becomes a minimum with a value $\neq 0$. We find that $J_0 < -\omega_0^2/\beta$ for $285 \leq g < 494$ and $995 \leq g < 1084$. In these two intervals the shape of the potential V_{eff} becomes a double-well and in the first interval of g , Q displays double resonance with the peak value $Q = 2$ while in the second interval of g , Q displays single resonance with the peak value less than 2. What will happen if X^* is chosen as $X^* \neq 0$? We answer for this for $\beta = 15$.

4.2. Potential with five wells ($\beta = 15$)

When $\beta = 15$ the potential is a five-well potential and is shown in Fig. 1c. We designate the middle well (centered at $x = 0$) as MW, the left-most well as LMW, the right-most well as RMW, the well lying between the middle-well and the left-most well as LWAMW (left-well adjacent to the middle-well) and the well lying between the middle-well and the right-most well as RWAMW. For $\beta = 15$ also the response amplitude exhibits a number of resonance peaks and it becomes 2 in the limit of $g \rightarrow \infty$. We compute Q for three different initial conditions. We choose these initial conditions as $\dot{x}(0) = 0$ and $x(0)$ as (i) the minimum of the MW potential ($x(0) = 0$), (ii) the minimum of the RWAMW ($x(0) = 5.88$) and (iii) the minimum of the RMW ($x(0) = 11.67$). Fig. 6a–c show the Q obtained as a function of g in the interval $[0, 250]$ for the above three initial conditions. The variations of the center of the orbit denoted as x_c corresponding to the subplots a–c are plotted in Fig. 6d–f. Fig. 6a is for the initial condition chosen in the MW. Corresponding to this case, in Fig. 6d $x_c = 0$ and $x(t)$ oscillates about $x_c = 0$. In Fig. 6e corresponding to the initial condition chosen in the RWAMW for $0 < g < 187$ $x_c = 5.88$. That is, $x(t)$ is confined to this well. As g increases from 0 the size of the orbit and the response amplitude $Q(\omega)$ increase from a small

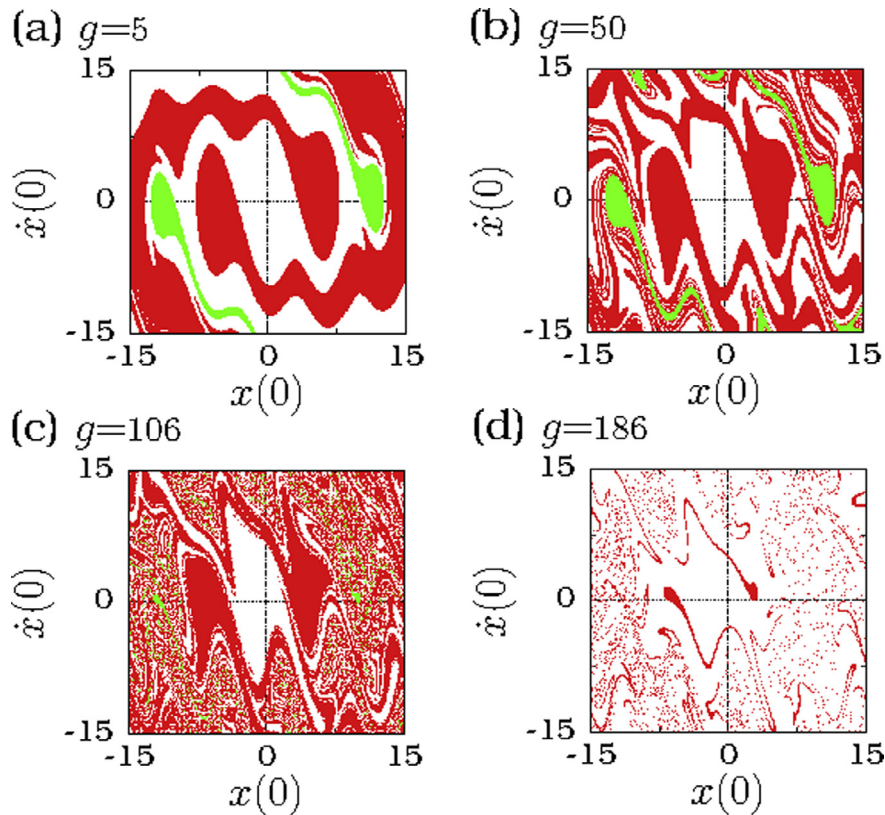


Fig. 7. Basin of attraction plots of the orbits confined to the different wells of the potential $V(x)$ of the system (2) for four values of g with $d = 0.5$, $f = 0.1$, $\omega_0^2 = 1$, $\omega = 1$, $\Omega = 10\omega$ and $\beta = 15$. The gray and black coloured regions correspond to the RMW (or LMW) and RWAMW (or LWAMW). The blank regions represents the basin of attraction of the orbit confined to MW. For details see the text.

value. This happens for $0 < g < 187$. At $g = 187$ the orbit is able to overcome the barrier between the MW and RWAMW. The orbit jumps to the MW and is confined to it. This is clear in Fig. 6e where x_c suddenly jumps to the value 0 at $g = 187$ and the value of Q also makes a jump from a higher value to the value 0.216. For further increase in g the value of Q follows the path of Q realized in Fig. 6a. Same result occurs if the initial condition is chosen as the minimum of the LWAMW.

Suppose the initial condition is $\dot{x}(0) = 0$ and $x(0)$ is the minimum of the RMW (or LMW). Then when g is varied from a small value the motion of the system is confined to this potential well for $0 < g < 107$. In this interval of g , Q increases from a small value. At $g = 107$ the Q value jumps from a higher value to a lower value as shown in Fig. 6c. This is because at this value of g the trajectory jumps to RWAMW and confined to that well. Consequently, in Fig. 6c we observe that x_c jumps from a value 11.67 to a value 5.88. Then for $g \geq 107$, Q and x_c follow the paths shown in Fig. 6b and c, respectively.

5. Basin of attraction

In Section 4 for $\beta = 15$ we have shown in Fig. 6 that for each value of g in the interval $0 < g < 107$ there are three distinct values of Q corresponding to the coexistence of the three distinct orbits confined to the MW, confined to the RWAMW (or LWAMW) and confined to the RMW (or LMW). In obtaining Fig. 6a–c we used three distinct initial conditions only. The orbit in the limit of $t \rightarrow \infty$ will be sensitive to initial conditions. Therefore, it is important to know the basin of attraction of each value of Q , that is each of the three distinct orbits. We computed basin of attraction of these three orbits for a range of values of g with $x(0) \in [-15, 15]$ and $\dot{x}(0) \in [-15, 15]$. This range of initial conditions is divided into number of grid points. Each grid point is treated as an initial condition. For each initial condition the Eq. (2) is integrated and after leaving sufficient transient the Q value of the long time orbit is calculated and the potential well within which the orbit lies is noted.

Fig. 7 shows the basin of attraction for the three orbits for four values of g . The gray coloured and black coloured grid points represent basin of attraction of the orbits confined to the RMW (or LMW) and RWAMW (or LWAMW) of the potential, respectively. The blank region represents the basin of attraction of the orbit confined to MW. For $g = 5$ the basin boundaries of the basin of attraction of the various orbits are smooth. As the value of g increases the complexity of the basin of attraction plot increases. This is evident from Fig. 7b and c corresponding to $g = 50$ and $g = 106$, respectively. For further

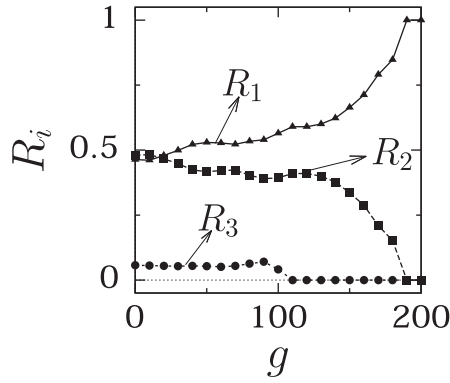


Fig. 8. Plot of R_i , $i = 1, 2, 3$ versus the control parameter g . Here $d = 0.5$, $f = 0.1$, $\omega_0^2 = 1$, $\omega = 1$, $\Omega = 10\omega$ and $\beta = 15$. For details see the text.

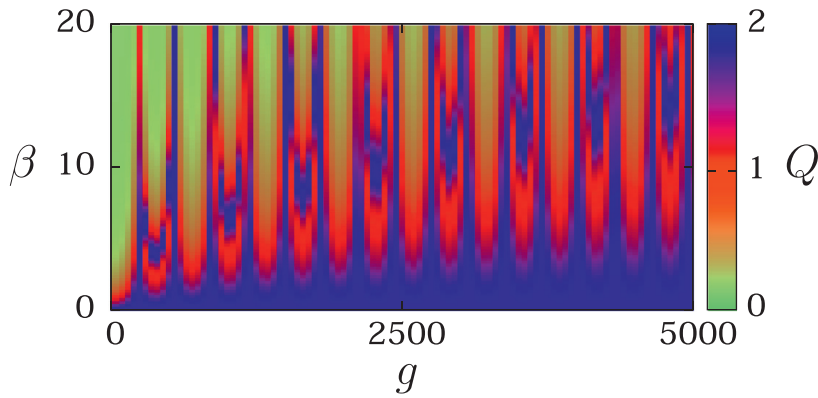


Fig. 9. Q as a function of β and g . The values of the other parameters are $d = 0.5$, $f = 0.1$, $\omega_0^2 = 1$, $\omega = 1$ and $\Omega = 10\omega$.

analysis we define the quantity R_i as

$$R_i = \frac{N_i}{N}, \tag{17}$$

where N is the total number of initial conditions and N_i is the number of initial conditions leading to the i th orbit. We designate $i = 1, 2$ and 3 for the orbits confined to MW, LWAMW (or RWAMW) and LMW (or RMW), respectively. Fig. 8 presents the variation of R_i with g . As g increases R_1 increases while R_2 and R_3 decrease. For $g \geq 107$ $R_3 = 0$ while $R_2 = 0$ for $g \geq 187$. R_1 becomes unity for $g \geq 187$. Finally, Fig. 9 shows colour code plot of variation of Q with the parameters β and g .

6. Conclusion

We considered a biharmonically driven oscillator with the potential given by Eq. (1). Depending upon the values of the parameters ω_0^2 and β , $V(x)$ admits odd number of wells. We explored the effect of shape of the potential on vibrational resonance. Using a theoretical method an analytical expression for the response amplitude $Q(\omega)$ is obtained. One interesting result is that for a fixed values of the parameters when the control parameter g is varied the response amplitude displays a number of resonance peaks and $Q(\omega) \rightarrow 2$ in the limit of $g \rightarrow \infty$. Whenever a resonance peak occurs due to the matching of ω_r with ω then $Q(\omega) = 1/(d\omega)$. Resonance is found to occur due to the local minimum of $|\omega_r^2 - \omega| \neq 0$. The effect of β is described. For systems with polynomial potentials $Q(\omega) \rightarrow 0$ as $g \rightarrow \infty$. In contrast to this in system (2) even for the single-well potential $Q(\omega)$ not decays to zero but approaches the limiting value $1/(d\omega)$. Investigation of other types of resonances in the system with the potential given by Eq. (1) may provide interesting results.

Acknowledgment

KA acknowledges the support from University Grants Commission (UGC), India in the form of UGC-Rajiv Gandhi National Fellowship. Financial support from the Spanish Ministry of Economy and Competitiveness under Project No. FIS2013-40653-P and Project No. FIS2016-76883-P is acknowledged.

References

- [1] Minorsky N. Nonlinear oscillations. New York: Van Nostrand; 1962.
- [2] Nayfeh AH, Mook DT. Nonlinear oscillations. New York: John Wiley & Sons; 1979.
- [3] Jordan DW, Smith P. Nonlinear ordinary differential equations: an introduction for scientists and engineers. Oxford: Oxford University Press; 2007.
- [4] Rajasekar S, Sanjuán MAF. Nonlinear resonances. Heidelberg: Springer; 2016.
- [5] Landau L, Lifshitz E. Mechanics. London: Pergamon; 1960.
- [6] Benzi R, Sutera A, Vulpiani A. The mechanism of stochastic resonance. *J Phys A* 1981;14:L453–7.
- [7] Ando B, Graziani S. Stochastic resonance: theory and applications. Dordrecht: Kluwer Academy Publishers; 2000.
- [8] Gang H, Ditzinger T, Ning CZ, Haken H. Stochastic resonance without external periodic force. *Phys Rev Lett* 1993;71:807–10.
- [9] Pikovsky AS, Kurths J. Coherence resonance in a noise-driven excitable system. *Phys Rev Lett* 1997;78:775–8.
- [10] Meerson B, Friédland L. Strong autoresonance excitation of Rydberg atoms: the Rydberg accelerator. *Phys Rev A* 1990;41:5233–6.
- [11] Manevitch LI, Kovaleva AS, Shepelev DS. Non-smooth approximations of the limiting phase trajectories for the duffing oscillator near 1:1 resonance. *Physica D* 2011;240:1–12.
- [12] Chialvo DR, Calvo O, Gonzalez DL, Piro O, Savino GV. Subharmonic stochastic synchronization and resonance in neuronal systems. *Phys Rev E* 2002;65:050902(R).
- [13] Rajamani S, Rajasekar S, Sanjuán MAF. Ghost-vibrational resonance. *Commun Nonlinear Sci Numer Simulat* 2014;19:4003–12.
- [14] Abirami K, Rajasekar S, Sanjuán MAF. Vibrational and ghost-vibrational resonance in a modified Chua's circuit model equation. *Int J Bifur Chaos* 2014;24:1430031.
- [15] Zambrano S, Casado JM, Sanjuán MAF. Chaos-induced resonant effects and its control. *Phys Lett A* 2007;366:428–32.
- [16] Landa PS, McClintock PVE. Vibrational resonance. *J Phys A* 2000;33:L433–8.
- [17] Gitterman M. Bistable oscillator driven by two periodic fields. *J Phys A* 2001;34:L355–7.
- [18] Blekhnman II, Landa PS. Conjugate resonances and bifurcations in nonlinear systems under biharmonic excitation. *Int J Non-Linear Mech* 2004;39:421–6.
- [19] Rajasekar S, Used J, Wagemakers A, Sanjuán MAF. Vibrational resonance in biological nonlinear maps. *Commun Nonlinear Sci Numer Simulat* 2012;17:3435–45.
- [20] Jeyakumari S, Chinnathambi V, Rajasekar S, Sanjuán MAF. Role of depth and location of minima of a double-well potential on vibrational resonance. *J Phys A* 2010;43:465101.
- [21] Chizhevsky VN, Smeu E, Giacomelli G. Experimental evidence of “vibrational resonance” in an optical system. *Phys Rev Lett* 2003;91:220602.
- [22] Chizhevsky VN, Giacomelli G. Improvement of signal-to-noise ratio in a bistable optical system: comparison between vibrational and stochastic resonance. *Phys Rev A* 2005;71:011801.
- [23] Chizhevsky VN, Giacomelli G. Experimental and theoretical study of vibrational resonance in a bistable system with asymmetry. *Phys Rev E* 2006;73:022103.
- [24] Baltanás JP, López L, Blekhnman II, Landa PS, Zaikin A, Kurths J, et al. Experimental evidence, numerics and theory of vibrational resonance in bistable systems. *Phys Rev E* 2003;67:066119.
- [25] Jeyakumari S, Chinnathambi V, Rajasekar S, Sanjuán MAF. Single and multiple vibrational resonance in a quintic oscillator with monostable potentials. *Phys Rev E* 2009;80:046608.
- [26] Jeyakumari S, Chinnathambi V, Rajasekar S, Sanjuán MAF. Vibrational resonance in an asymmetric duffing oscillator. *Int J Bifur Chaos* 2011;21:275–86.
- [27] Rajasekar S, Abirami K, Sanjuán MAF. Novel vibrational resonance in multistable systems. *Chaos* 2011;21:033106.
- [28] Abirami K, Rajasekar S, Sanjuán MAF. Vibrational resonance in the Morse oscillator. *Pramana J Phys* 2013;81:127–41.
- [29] Ullner E, Zaikin A, Garcia-Ojalvo J, Bascones R, Kurths J. Vibrational resonance and vibrational propagation in excitable systems. *Phys Lett A* 2003;312:348–54.
- [30] Abirami K, Rajasekar S, Sanjuán MAF. Vibrational resonance in a signum nonlinearity system. *J Discontinuity, Nonlinearity Complexity* 2016;5:43–58.
- [31] Mueller F, Heugel S, Wang LJ. Optomechanical stochastic resonance in a macroscopic torsion oscillator. *Phys Rev A* 2009;79:031804(R).
- [32] Boas ML. Mathematical methods in the physical science. New Delhi: Wiley; 2006.
- [33] Tang KT. Mathematical methods for engineers and scientists: Fourier analysis, partial differential equations and variational methods. Heidelberg: Springer; 2007.